Echoes—How to Generate, Recognize, Use or Avoid Them in MR-Imaging Sequences
Part I: Fundamental and Not So Fundamental Properties of Spin Echoes

Jürgen Hennig

Radiologische Klinik
Abt. Röntgendiagnostik
Hugstetterstr. 55
78 Freiburg
Germany

Spin echoes have been known since 1950. Although their formal description by use of the Bloch equations is straightforward, it does not lead to an intuitive understanding of their behavior except for the special cases of 180° or 90° pulses, especially when many pulses are applied before the magnetization has returned into thermal equilibrium. The extended-phase-graph algorithm, which takes into account that the total magnetization in spin-echo sequences is a superposition of many isochromats, allows the recognition of all possible echo signals in arbitrary pulse sequences. Its application to multi-echo sequences leads to a number of surprising results. It can be demonstrated that refocusing pulses with flip angles much lower than 180° generate an unexpectedly high signal intensity after a few echo periods. Apart from leading to a simple algorithm for the exact calculation of echo intensities in arbitrary multi-pulse sequences, the phase-graph algorithm leads to a simple understanding of the contrast behavior of different gradient echo sequences and gives a rational means for the design of MR-imaging sequences that are free from spurious echoes.

INTRODUCTION

The concept of spin echoes was presented in 1950 by E. L. Hahn in a remarkable paper that contains almost everything there is to know about the behavior of uncoupled spin-½ nuclei (*1*). Since then, the ability to realign incoherent magnetization vectors by a 180° refocusing pulse has been one of the textbook basics of NMR. Innumerable students have seen their teachers wave their arms and turn around their (vertical) axis to illustrate this phenomenon. It is interesting that the very simplicity and clarity of the vector model for the explanation of this primary spin echo seems to preclude our understanding of other echoes, such as those generated by 90°

refocusing pulses. Two diverging vectors just do not seem to converge after only a half-turn. As a consequence, irrational spirits of magnetic resonance often are invoked to explain the existence of such echoes or their even more esoteric relatives, the stimulated echoes.

Before continuing, it is necessary to state that nothing but rotations of vectors in space will be necessary to understand this article. Not even an understanding of relatively benign effects like J-coupling will be required; I will deal exclusively with uncoupled spin-½ particles (which about covers my expertise).

In Part I, I present a comprehensive explanation of the echo phenomenon and introduce a simple and illustrative model that can be used to trace and calculate the amplitude of all possible echoes generated by any sequence of radio-frequency (rf) pulses. Then I will demonstrate how easy it is to calculate the amplitudes of practical multi-echo sequences, where the refocusing flip angle never is exactly 180? Because multi-echo sequences with constant echo spacing are the simplest multi-pulse sequences, I will use them to illustrate some features of echo formation beyond the mere practical aspects of the design and optimization of such an experiment. Here the reader must expect to be confronted with strange things like echo sequences with increasing echo amplitudes or even echo solitons, which seem to roll on forever.

More practical aspects of MR-imaging experiments are described in Part II. After the consequences of echo formation for a multi-echo imaging experiment are discussed, I will demonstrate how easy it is to describe the contrast behavior of gradient echo sequences if they are regarded as multi-echo sequences (which they indeed are). Finally, some basic traps in any periodic NMR experiment, such as an MR-imaging experiment, are given.

THEORY OF ECHOES

Echo Formation

Transverse magnetization is generated by a hard 90° pulse, which rotates all z magnetization into the transverse plane. If the B_1 field of the pulse is aligned along the y axis of the rotating frame, then the transverse magnetization after the pulse will be directed into the x direction according to the generally accepted right-hand rule. Due to magnetic-field inhomogeneities over the probe, nuclei at different locations will see a slightly different B_0 field and will therefore precess with a slightly different Larmor frequency. If two such spins are chosen at random, the dephasing can be visualized by vectors lagging behind or advancing in the rotating frame given by the reference frequency. The observed signal that is the sum of all vectors will consequently be reduced on a time scale given by this loss of coherence. If a 180° pulse with phase x is applied after a certain interval, both vectors will be rotated by 180° around the x axis. It is now easy to see that both vectors will coincide on the x axis after the same time interval: A spin echo has been formed (Fig. 1).
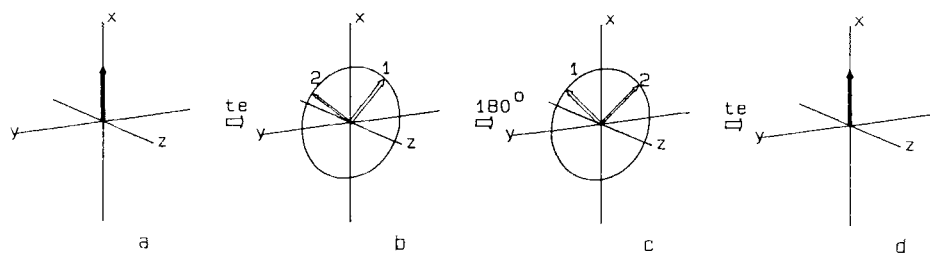

Figure 1. Principle of Refocusing by a 180° Pulse. (a) After excitation by a y pulse, all z magnetization is converted into x magnetization. (b) After an interval t_e, two vectors corresponding to isochromats with different Larmor frequencies are somewhat dephased. (c) A 180° pulse (x) negates the y components of the two vectors. (d) After another interval, both vectors will be realigned on the x axis.

126

This was the easy part. Now what about echo formation by a 90° pulse? To understand this, we should look at the transverse magnetization after a time t_e when all spins are totally dephased in the transverse plane such that the tips of all vectors are equally distributed over a circle (Fig. 2b). If now a 90° pulse is applied, the whole circle will be rotated into the zy plane
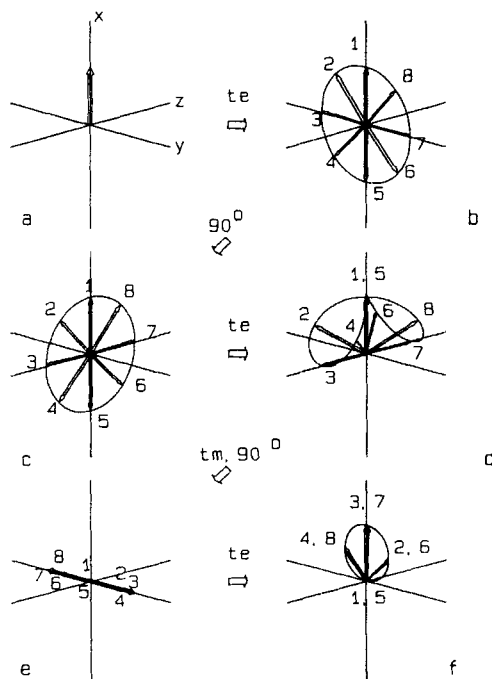

Figure 2. Principle of Refocusing by a 90° Pulse. (b) The x magnetization created by the excitation pulse dephases totally in the xy plane. (c) The dephased spin ensemble is rotated by a 90° pulse into the xz plane. (d) After another time t_e, all vectors will be located on the same side of the yz plane. (e) Only the z components of all vectors remain after T_2 relaxation, which can then be converted into y magnetization by another 90° pulse. (f) After a further interval t_e, all vectors will again be located on the same side of the yz plane.

(Fig. 2c). Let us now select eight isochromats represented by eight vectors spaced at 45° along this circle as representative of this equal distribution. To follow their path for the next interval t_e, it must be kept in mind that the phase angle by which each vector will rotate in the transverse plane is the same as before the pulse (we neglect such time-variable processes as diffusion, motion, or magnetic-field variations for the moment). That means vector 1 will stay in place, vector 2 will travel 45°, and so on. The result shows that the vectors are not aligned on the y axis, as they are with a 180° refocusing pulse, but that they lie all on the same side of the xz plane (Fig. 2d). Their sum will therefore produce a non-zero contribution in the x direction. The symmetry of the pattern that results from filling the gaps between the eight vectors shows that the resultant will be located exactly on the x axis. For all of those who have difficulty visualizing the curve in Fig. 2d, it can be described as a soft "figure 8" that rests on the surface of a sphere. Salvador Dali would have loved it!

Because the effort already has been made to prepare the spin system in the described manner, we might as well ask what happens with the z components of the magnetization vectors. These will stay on the z axis until T_1 relaxation has brought them back to equilibrium. It should be noted that the size of these z components depends on the phase of each vector at the time of the refocusing pulse. Vectors 1 and 5 represented pure transverse magnetization after the refocusing pulse. Because the different phase angles of the vectors are a consequence of magnetic-field inhomogeneity, a spatial variation of z magnetization is thus created. If another 90° pulse is applied after a time t_m long after T_2 relaxation has annihilated all signal from the first echo, this z magnetization will be awakened to form transverse magnetization (Fig. 2e).

After another interval t_e, each vector will have traveled the same phase angle as in the interval before the refocusing pulse. Figure 2f demonstrates that again all vectors will be on the same side of the xz plane: A stimulated echo has been formed.

If multiple refocusing pulses are applied at times $2 \cdot (n - 1) \cdot t_e$ after excitation, then the pattern generated by the tips of all magnetization vectors looks more and more complex (Fig. 3).
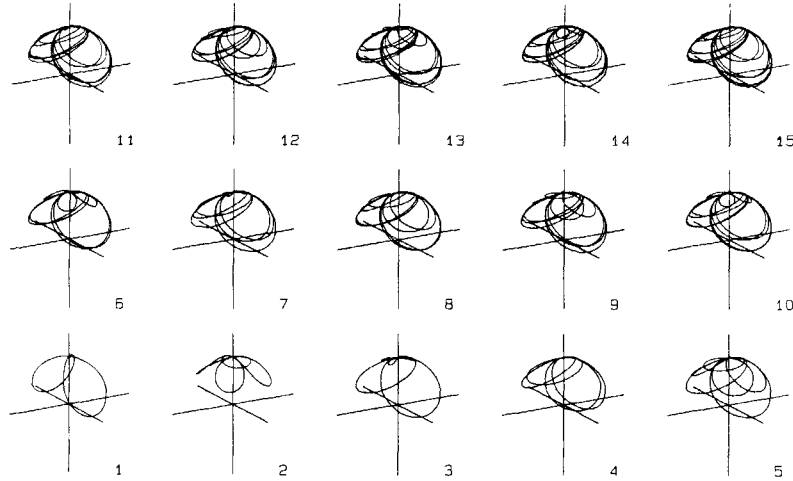

Figure 3. Evolution of a spin system undergoing a multi-echo experiment with 90° refocusing pulses. The tips of all magnetization vectors are shown at the times of echo generation in each refocusing period.

The fact that at each echo time $2 \cdot n \cdot t_e$ all magnetization still lies on the same side of the xy plane tells us that these echoes will have non-zero intensities. The calculation of these intensities appears to be quite a formidable task, which we will not undertake now.

A comparison of a 90-90 echo with a 90-180 echo reveals an important difference: Every vector starting on the x axis after excitation will be brought back to the x axis if a spin echo is formed by a 180° pulse. This means that *any* distribution of spins with different Larmor frequencies will lead to echo formation. This is not true for the formation of the 90-90 echo and the stimulated echo. Here it is essential that the vectors are *evenly* distributed over the transverse plane at the time of the refocusing pulse. Taking only two vectors (for example, 3 and 7) would not lead us to expect echo formation, which is the reason the explanation of the refocusing mechanism using two arms fails miserably. An octopus would have less trouble understanding a 90-90 echo. This requirement of an equal distribution of spins for the formation of 90-90 echoes or stimulated echoes is the reason the art of forming echoes has practically fallen into oblivion during the 40 years since Hahn's article: State-of-the-art NMR spectrometers have such excellent magnetic-field homogeneities that this condition for the formation of more interesting echoes just is not met. This is very different in MR-imaging systems where the magnetic-field gradients used for encoding spatial information generate quite some dephasing of the spins over the observed volume. To give an idea of the amount of dephasing encountered under practical MR-imaging conditions, let us take a 256 x 256 data acquisition matrix. Each projection step will contain 256 complex data points under the read gradient. Using the sampling theorem, this means that the difference in phase angle between the spins located in the outermost voxels covered by the acquisition band-width will be 256 x 180°, or 128 full turns. That means that at the time of the refocusing pulse, the minimum dephasing will be just these 128 turns if no negative gradient lobes are used for prefocusing. It is no overstatement to talk about the loss of coherence in this context. The fact that the phases of the spins are so hopelessly scrambled at the time of rf pulses also sheds some doubt whether the vector model that uses pure magnetization vectors really is an appropriate tool for tracing the observed signals.

128

In the following section, the standard algorithm for the calculation of echo amplitudes will be shown, and then a much simpler method will be given.

Extended-Phase-Graph Algorithm

The calculation below closely follows the formalism given by Woessner (2). The effect of an rf pulse with phase x applied to the pure magnetizations M_x, M_y, and M_z can be treated as a simple rotation around the x axis with the flip angle α. The magnetizations M_x^+, M_y^+, and M_z^+ immediately after the pulse will then be given by

$$M_x^+ = M_x \tag{1}$$

$$M_y^+ = M_y \cdot \cos\alpha - M_x \sin\alpha \tag{2}$$

and

$$M_z^+ = M_y \cdot \sin\alpha + M_z \cos\alpha \tag{3}$$

Now the complex magnetization F and its complex conjugate F* are introduced, given by

$$F = M_x + iM_y \tag{4}$$

and

$$F^* = M_x - iM_y \tag{5}$$

Substitution into Eq. [1] through Eq. [3] leads to

$$F^+ = F \cdot \cos^2(\alpha/2) + F^* \cdot \sin^2(\alpha/2) - i \cdot M_z \cdot \sin(\alpha) \tag{6}$$

and

$$M_z^+ = M_z \cdot \cos\alpha - \tfrac{1}{2} \cdot i \cdot (F - F^*) \cdot \sin\alpha \tag{7}$$

It should be noted that Eqs. [6] and [7] follow directly from Eqs. [1], [2], and [3] without anything other than formal substitution and the application of some formulas for the conversion of sums of trigonometric terms. The x and y components of each isochromat and its time evolution after the pulse must be calculated to calculate the amplitude. Vector addition at the echo time $2 \cdot t_e$ will then yield the echo amplitude. Carrying out this calculation can be quite tedious depending on the distribution of Larmor frequencies for a given sample in a given space-dependent magnetic field. To trace all of these vectors is especially annoying in view of the fact that all of these millions of calculation steps must be performed to get one single number that describes the echo amplitude. Although the calculation by itself constitutes no tremendous problem for a moderately fast computer — the graphs shown in Fig. 3 took only a few seconds of computation time — such a brute force attempt does not give any significant insight about the behavior of a spin system exposed to multiple rf pulses. A method that reduces the amount of number crunching and gives us some understanding of what is going on would therefore be extremely welcome.

Under the condition that all transverse magnetization vectors before each pulse shall be totally defocused, such an algorithm can easily be found (3). Let us call the particular configuration of magnetization vectors immediately before an rf pulse F_1. The actual x and y components of each vector are unknown. A pictorial representation of F_1 is the circle described by the tips of vectors in Fig. 2b. Although the transverse magnetization given by the sum of all vectors is zero because of total dephasing, all transverse magnetization at the time of the pulse has entered this configuration, whose population is therefore set to 1 — or to $\sin(\alpha)$ for an arbitrary flip angle α of the excitation pulse.

As a pendant to F_1, we can define a second configuration F_1^*, which can be created from F_1 by inversion of the y components of each vector. In other words, F_1^* is the mirror image of F_1 with the xz plane as the mirror. Because all transverse magnetization before the pulse is contained in F_1, the population of F_1^* before the pulse will be zero. It can be seen immediately

from Fig. 1 that all magnetization will be transferred from F_1 to F_1^* by a 180° refocusing pulse. The echo intensity after the pulse is consequently given by the population of F_1^* after the pulse.

Because F_1 is the configuration of the dephased transverse magnetization before the pulse, every magnetization contained in F_1 after the pulse will dephase further into a configuration F_2 before the next pulse. Appropriate configurations Z_n and Z_n^* can be defined to describe the spatial variable distribution of z magnetization leading to the formation of the stimulated echo. Equations [1] through [5] can now be used as parameter equations for the different configurations F_n, F_n^*, Z_n, and Z_n^*, which are given by

$$F_n = \int_{\omega - \Delta\omega}^{\omega + \Delta\omega} (M_x \cdot \cos\omega \cdot t_{en} + M_y \cdot \sin\omega \cdot t_{en}) d\omega \qquad [8]$$

$$F_n^* = \int_{\omega - \Delta\omega}^{\omega + \Delta\omega} (M_x \cdot \cos\omega \cdot t_{en} - M_y \cdot \sin\omega \cdot t_{en}) d\omega \qquad [9]$$

$$Z_n = i \cdot \int_{\omega - \Delta\omega}^{\omega + \Delta\omega} (M_x \cdot \cos\omega \cdot t_{en} + M_y \cdot \sin\omega \cdot t_{en}) d\omega \qquad [10]$$

$$Z_n^* = i \cdot \int_{\omega - \Delta\omega}^{\omega + \Delta\omega} (M_x \cdot \cos\omega \cdot t_{en} - M_y \cdot \sin\omega \cdot t_{en}) d\omega \qquad [11]$$

$2 \cdot \Delta\omega \cdot t_{en}$ must be at least 360° to ensure full dephasing. For a multi-echo experiment with equally spaced refocusing pulses, a pictorial representation for the states F_n, F_n^*, Z_n, and Z_n^* is given by Fig. 4. Because z magnetization is always located on the z axis, it is advisable to regard
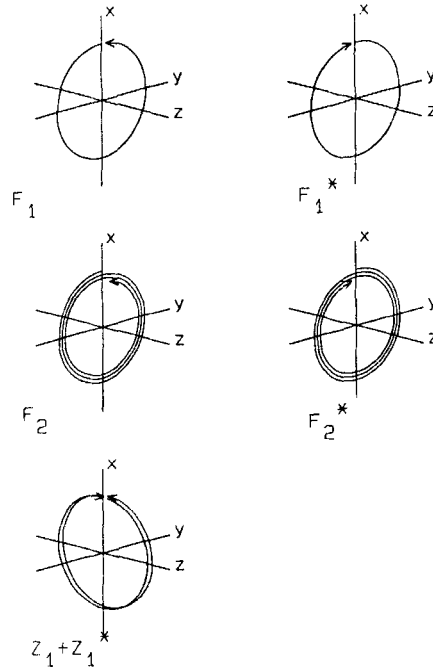

Figure 4. The Configurations F_1, F_1^*, F_3, F_3^*, and $Z_1 + Z_1^*$. The arrows indicate the sense of rotation with increasing frequency offset to the rotating reference frame. The circular polarized configurations Z_1 and Z_1^* always occur in pairs to represent the linear polarized configurations of z magnetization.

130

the combination of the two Z terms rather than each term alone. This is equivalent to the description of a linearly polarized wave as the sum of two counter-rotating, circular polarized waves.

All that is necessary for the calculation of the echo amplitudes in any arbitrary pulse sequence is to calculate the flow of magnetization between the different possible configurations. The echo amplitude will then be given by the population of the configuration leading to echo formation, which is F_1^* for the spin-echo experiment.

A simple way to keep track of all configurations involved is to use an extended-phase graph, which looks like Fig. 5 for a multi-echo experiment. Comparing Fig. 5 with Fig. 3, it is obvious that a tremendous amount of unnecessary detail has been removed.
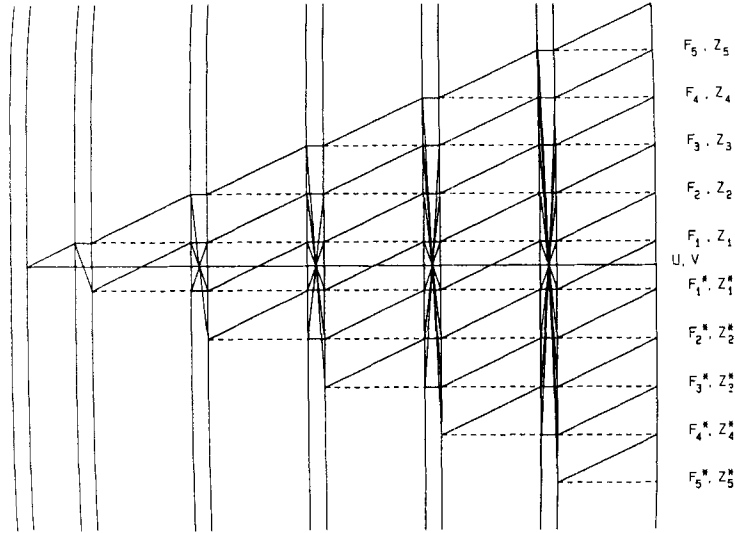

Figure 5. Extended-phase graph for a Carr-Purcell-Meiboom-Gill (CPMG) multi-echo sequence. Pulses are represented by two closely spaced vertical lines. The mixing between configurations F_n, F_n^*, Z_n, and Z_n^* with identical n is shown by the lines that connect these states. Time evolution of transverse magnetization is shown by solid lines between pulses; the dotted horizontal lines represent configurations of z magnetization.

If the phase of the rf pulses is such that echoes with different phases might arise, the number of configurations must be enlarged to include F_{nx}, F_{nx}^*, F_{ny}, F_{ny}^*, and the corresponding Z states as a basis. The echo amplitudes E_n will then be given by

$$E_n = \sqrt{F_{1x}^{*2} + F_{1y}^{*2}} \qquad [12]$$

If the phase of all refocusing pulses is the same, then the phase of all echoes will be the same, and the reduced set using F_n, F_n^*, Z_n, and Z_n^* is sufficient. Negative echo amplitudes are treated by allowing negative values for the populations of the corresponding configurations.

The identity of the echo amplitudes with the population of the configurations F_n^* is the reason that the magnetization vectors in each configuration must be totally dephased. In all other cases, E_n will be a more or less complicated function of F_n and F_n^*. The exact computation of this function requires the knowledge of the distribution of the phase of the magnetization vectors, which means we are back to square one and might as well start computing the Bloch equations for millions of isochromats.

Formally the time evolution and the effect of each pulse in the phase-graph algorithm can be described simply by transition matrices. The effect of the pulse is described by

131

$$M^+ = M \cdot T_p$$

where

$$M = (M_x \; M_y \; M_z \; F_1 \; F_1^* \; Z_1 \; Z_1^* \; F_2 \; F_2^* \; ...)$$

describes the total magnetization before the pulse, and T_p represents the transition matrix, given by

$$T_p = \begin{bmatrix} T_0 & & & & \\ & T_1 & & & \\ & & T_1 & & \\ & & & T_1 & \\ & & & & \cdot \\ & & & & & \cdot \end{bmatrix} \qquad [13]$$

It is useful to retain the usual rotation matrix for the description of the effect of the pulse on pure magnetizations. For an x pulse, this is given by

$$T_0 = \begin{bmatrix} 1 & 0 & 0 \\ 0 & \cos\alpha & -\sin\alpha \\ 0 & \sin\alpha & \cos\alpha \end{bmatrix} \qquad [14]$$

For a certain n, the matrix T_1 linking the four possible configurations F_n, F_n^*, Z_n, and Z_n^* before and after the pulse with flip angle α is given by

$$T_1 = \begin{bmatrix} \cos^2\alpha/2 & \sin^2\alpha/2 & \sin\alpha & 0 \\ \sin^2\alpha/2 & \cos^2\alpha/2 & 0 & \sin\alpha \\ \tfrac{1}{2}\sin\alpha & -\tfrac{1}{2}\sin\alpha & \cos\alpha & 0 \\ -\tfrac{1}{2}\sin\alpha & \tfrac{1}{2}\sin\alpha & 0 & \cos\alpha \end{bmatrix} \qquad [15]$$

The evolution of magnetization between pulses can be described following the extended-phase graph for the particular pulse sequence. Relaxation or diffusion terms can be introduced in the time evolution as described in Reference 3 for a multi-echo experiment.

Some Exercises Using the Extended-Phase-Graph Formalism

The newly defined configurations constitute no orthonormal basis for the matrix calculations. Consequently, the condition of conserving the total amount of magnetization, which for a basis of pure magnetization vectors M_x, M_y, and M_z is given by

$$M_x^2 + M_y^2 + M_z^2 = \text{const.} = 1 \qquad [16]$$

after normalization is substituted by

$$\sum_{n=1}^{m} F_n + F_n^* + Z_n + Z_n^* = \text{const.} = 1 \qquad [17]$$

From Eq. [13] also follows

$$Z_n + Z_n^* = 0 \qquad [18]$$

as a consequence of the fact that to represent linear z magnetization, the populations of the two counter-rotating configurations Z_n and Z_n^* must be equally opposite.

It should be noted that conservation of the total amount of magnetization does not imply that any subset of all configurations, such as ΣF_n^*, is normalized. The sum of the amplitudes of all echoes occurring after the last pulse might very well be greater than 1, contrary to some of the fuzzy notions one encounters in discussions of this subject. As a trivial example, it is easy to calculate from Eq. [15] that the sum of all echoes generated by a three-pulse sequence with flip angles $90(y) - 120(x) - 120(x)$ is 1.125. This does not mean that a signal is created from nothing but simply is a consequence of the fact that the same spins can contribute to more than one signal.

It is of course trivial that no single population can be larger than 1, which is just another way to say that no configuration can contain more than all magnetization. The maximum number of signals that can be created by a given number of pulses can be calculated easily by induction: From Fig. 5, it is immediately apparent that the total numbers T_n and Z_n of transverse and longitudinal configurations after the nth pulse are given by

$$T_n = 2 \cdot T_{n-1} + Z_{n-1} + 1 \tag{19}$$

and

$$Z_n = 2 \cdot T_{n-1} + Z_{n-1} \tag{20}$$

This immediately leads to

$$T_n = 3 \cdot T_{n-1}$$

or

$$T_n = 3^{n-1}$$

with T_0 and Z_0 equal to 0.

Using the mirror symmetry of the number of states F_n and F_n^*, the number of echoes E_n is calculated as

$$E_n = (3^{n-1} - 1)/2 \tag{21}$$

The maximum number of echoes can of course be generated only if no F_n, F_n^*, Z_n, or Z_n^* is identical to another F_m, F_m^*, Z_m, or Z_m^*.

A simple way to achieve this is to increase the time t_n between pulses such that F_n^* leads to a new state F_{n+1} before the next pulse, as shown in Fig. 6a. It is easy to see that for this case $t_n = T_n \cdot t_0$, where t_0 is the basic time increment. With 100 pulses we can thus create a maximum number of $0,5 \cdot 3^{99}$ echoes. Using the sequence in Fig. 6a, this would take about $3^{99} \cdot t_0$, which is rather long compared with the relaxation times T_2 and T_1 for any practical value of t_0. The total universe including this paper will have vanished into oblivion long before the arrival of the last echo. We can of course turn the timing of pulses around by applying each pulse only $(1 + n)/n \cdot t_0$ after the preceding one, which leads to a somewhat nested appearance of the echo formation pathways (Fig. 6b). Then, however, we run into the problem that the time difference between the nth and the $(n + 1)^{th}$ pulse must be as short as $2 \cdot 3^{-99} \cdot t_0$, which constitutes some practical problems. Wrapping this argument together, it can be seen that only a tiny fraction of the possible maximum number of echoes will be formed. This is a comforting thought, because even for the modest number of 10^{20} echoes that could be generated by a sequence of only 44 pulses, we would otherwise have to imagine a single spin to form an echo with itself because 10^{20} is about the order of magnitude of the number of observable spins in a typical NMR experiment.

The reason this point of no apparent practical significance is being stressed is to demonstrate that even for moderate regularity of the timing of a multi-pulse sequence, a vast redundancy of configurations must be expected. If the signal amplitudes are calculated using the conventional formalism of tracing each pathway leading to the formation, then all possible pathways must be calculated, and the results must be combined afterwards. This requires the computation of all 3^{99} pathways leading to echo formation for a sequence of 100 pulses.
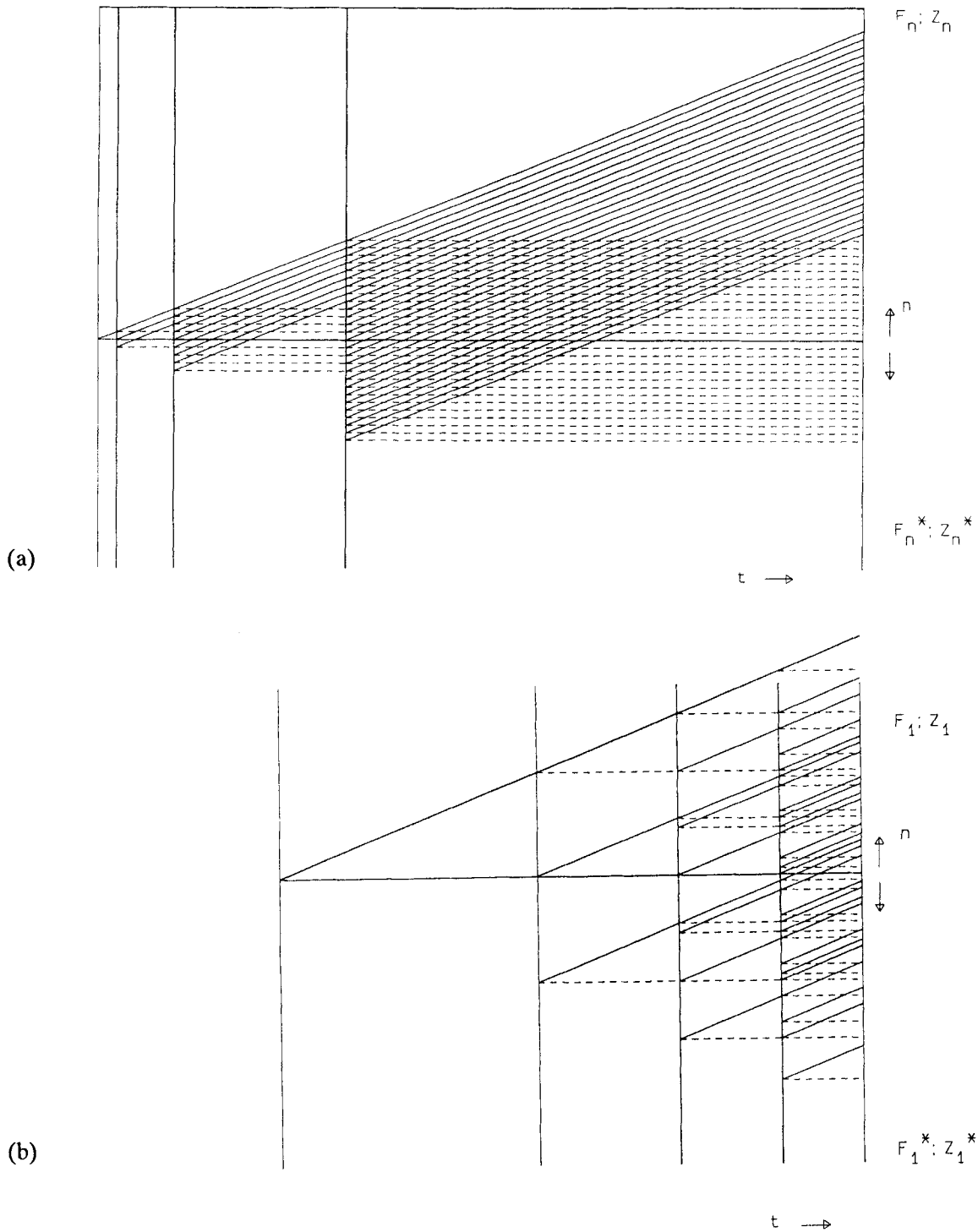
133

Figure 6. (a) Pulse sequence for the generation of the maximum number of different configurations by increasing the pulse spacing. Pulses are represented by single vertical lines. (b) A possible timing sequence for a decreasing pulse spacing.

Using the matrix formalism described above, and observing redundant configurations, the number of calculation steps can be reduced from 3^n to n^2 or even n, depending on the periodicity of the pulse sequence. As will be shown next, even multi-echo experiments with hundreds of pulses that would require astronomical effort to calculate with standard methods are possible.

MULTI-ECHO SEQUENCES

A conventional multi-echo sequence uses a 90° excitation pulse followed by a series of equally spaced 180° pulses such that an echo occurs in the center of the time interval between two refocusing pulses. If such an experiment is performed using hard pulses with exact flip angles, then the signal decay will be governed by the relaxation time T_2 and diffusion alone, where the diffusion term is significant only in samples with a large magnetic-field gradient. After the first proposal to measure the relaxation time with this method, several papers have been presented dealing with the problem, how nonperfect pulses affect the result of such an experiment, and how the expected errors can be minimized (4). These have led to the well-known CPMG sequence, where the phase of all the refocusing pulses is the same and orthogonal to the phase of the excitation pulse (5). Figure 5 shows the extended-phase graph for this sequence. It demonstrates that due to the periodicity of the timing, the number of different configurations grows only linear with the number of pulses. The calculation of the 50th echo therefore requires only the computation of the populations of 200 configurations by iterative application of the above matrix formalism rather than the calculation of some 10^{23} different refocusing pathways.

The reflow of magnetization into the echo *via* configurations with larger dephasing partially compensates or — as will be seen shortly — even overcompensates for the signal loss by $\sin^2(\alpha/2)$ when refocusing pulses with flip angles of less than 180° are applied. If the phase of the refocusing pulses and the excitation pulses is the same, then the sign of the primary echoes alternates from one refocusing pulse to the next. This leads to a sign reversal in the transition matrices for the effect of the refocusing pulse. It is easy to see that this sign reversal leads to some destructive interference of echoes generated *via* different pathways. The resulting echo amplitudes neglecting relaxation as a function of different refocusing flip angles are shown in Fig. 7 for both cases. It is immediately apparent that the CPMG sequence (Fig. 7b) yields more
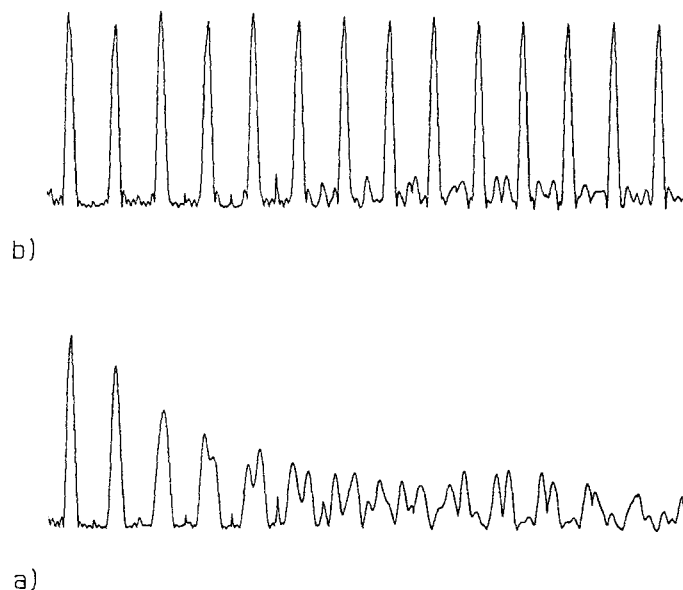

b)

a)

Figure 7. Fourteen echoes of a spin-echo sequence (a) with nominal 180° refocusing pulses and identical phases of the excitation pulse and the refocusing pulses and (b) with a CPMG sequence, where the phase of the excitation pulses is orthogonal to that of the refocusing pulses. Gaussian pulse-shapes were being used under a slice-selection gradient in the direction of the read gradient. The amplitude of the time domain signal is displayed. The pulse strength was adjusted to maximize the first echo.

signal due to the constructive interference of all refocusing pathways (5). For T_2 calculations, it should be noted that some of the signal will have been generated *via* Z configurations. The echo amplitudes will then depend not only on T_2, but also on T_1 and, most important, on the flip

135

angle. Figure 8 shows that — neglecting relaxation — a steady state of the echo amplitudes will be reached after a few refocusing periods. This means that even a flip angle as low as 30° will apparently refocus all magnetization observed in the preceding refocusing period, behavior that is commonly attributed exclusively to pure 180° pulses. Because this steady state appears to be quite remarkable, it will be discussed in more detail in the next section (the reading of which is not essential for the understanding of the more practical issues discussed in Part II of this paper).
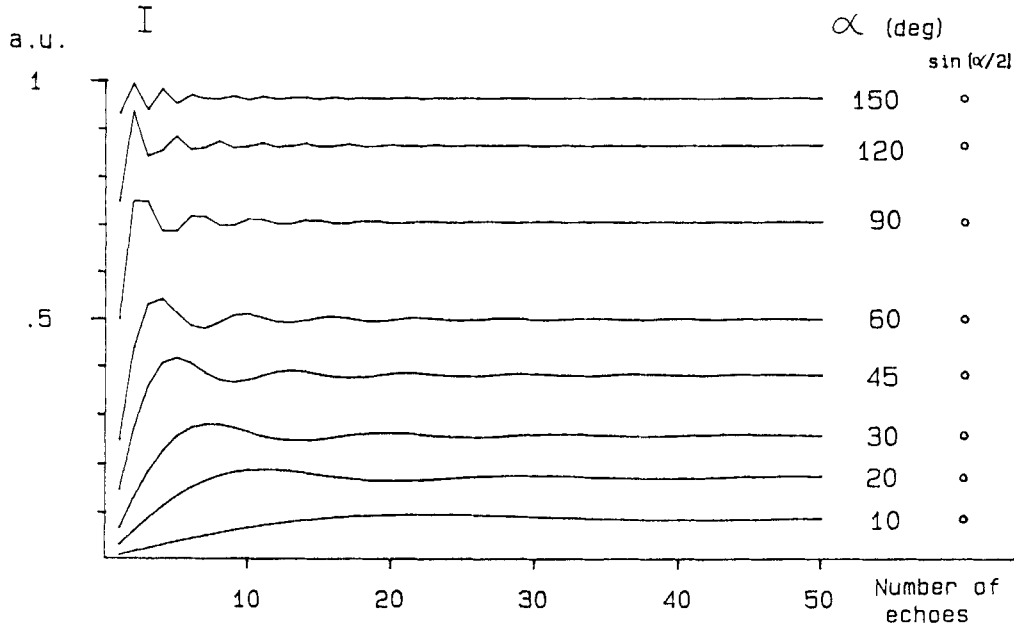
Figure 8. Calculated signal intensities of a multi-echo sequence for different values for the refocusing flip angle α. The open circles at the right side of each graph correspond to the steady-state value of $\sin(\alpha/2)$.

The Steady State of Echoes

Figure 8 is an illustration of the fact that the commonly used relationship between the intensities of subsequent echoes given by

$$E_n = E_{n-1} \cdot \sin^2(\alpha/2) \qquad [22]$$

is valid only for the refocusing of pure transverse magnetization. As soon as other configurations must be accounted for, Eq. [22] must be substituted with

$$E_n = E_{n-1} \cdot \sin^2(\alpha/2) + b_1 \cdot \cos^2(\alpha/2) - c_1 \cdot \sin(\alpha) \qquad [23]$$

This follows from the phase diagram (Fig. 5), which demonstrates that every signal is being generated from magnetization contained in one of the three configurations F_1, F_1^*, and Z_1^* before the refocusing pulse. The terms b_1 and c_1 are the populations of F_1^* and Z_1, respectively.

When no Z configuraton is present, Eq. [23] is reduced to the trivial statement that whenever E_{n-1} is larger than b_1, E_n will be maximum for a 180° refocusing pulse; if b_1 is larger than E_n, it is best to let this magnetization pass through without applying any pulse ($\alpha = 0$). With non-zero c_1, the situation becomes more interesting. Whereas Eq. [23] shows that for $\alpha = 180°$, E_n will always be equal to E_{n-1}, it is also easy to show that for any flip angle α, E_n can be made equal to E_{n-1} by choosing appropriate values for b_1 and c_1. That means any refocusing pulse can be made to generate something that looks like a fully refocused echo!

A thorough discussion of the steady state is a little bit more demanding. I will therefore only sketch the argument for the special case of $\alpha = 90°$. Table 1 gives the time evolution of the coefficients of F_n, F_n^*, Z_n, and Z_n^* for $\alpha = 90°$, where a_1 is identical to the echo amplitude E_{n-1} in the previous refocusing period.

TABLE 1

Evolution of Populations Between Two Refocusing Pulses in the Steady State

Configuration	Populations		
	Before Pulse	After Pulse	After Time Evolution
F_1	a_1	$a_1/2 + b_1/2 - c_1$	$a_1 = a_1/2 + b_1/2 + c_1$ [24]
F_1^*	b_1	$a_1/2 + b_1/2 + c_1$	$b_1 = a_2/2 + b_2/2 + c_2$ [25]
Z_1	c_1	$-a_1/2 + b_1/2$	$c_1 = -a_1/2 + b_1/2$ [26]
F_2	a_2	$a_2/2 + b_2/2 - c_2$	$a_2 = a_1/2 + b_1/2 - c_1$ [27]
F_2^*	b_2	$a_2/2 + b_2/2 + c_2$	$b_2 = a_3/2 + b_3/2 - c_3$ [28]
Z_2	c_2	$-a_2/2 + b_2/2$	$c_2 = -a_2/2 + b_2/2$ [29]
F_3	a_3	$a_3/2 + b_3/2 - c_3$	$a_3 = a_2/2 + b_2/2 - c_2$ [30]

It has already been pointed out that the population of all Z_n^* configurations is the inverse of that of the Z_n configurations. If we combine Eq. [24] and Eq. [26], it follows that the populations of $F_1 + Z_1^*$ remain constant even if no steady-state conditions exist. If we start with a 90° excitation pulse and normalize the initial transverse magnetization to 1, this leads to the additional equation

$$c_1 = a_1 - 1 \qquad [31]$$

Although half of the magnetization vanishes at every pulse into configurations with higher incoherence, there will always be a high population of the basic states F_1, F_1^*, Z_1, and Z_1^* available that can be used for subsequent signal generation.

Linear combination of Eqs. [24] through [31] leads to the following:

$$b_1 = 3 \cdot a_1 - 2$$

$$c_1 = a_1 - 1$$

$$a_2 = b_1 = 3 \cdot a_1 - 2$$

$$b_2 = a_3$$

$$c_2 = \tfrac{1}{2}(a_3 - 3 \cdot a_1 + 2) \qquad [32]$$

An infinite number of possible solutions exists even for the condition that the population of all configurations (and not only that of F_1^* after each pulse) is in a steady state.

The term a_3 describes the amount of magnetization that is exchanged between configurations with $n \leq 2$ and those with higher n. If this term is set to be zero, then the configurations with $n \leq 2$ become self-consistent, and steady-state solutions can be found for those configurations alone. From Eq. [32] follows then

$$b_1 = 3 \cdot a_1 - 2$$

$$c_1 = a_1 - 1$$

$$a_2 = b_1 = 3 \cdot a_1 - 2$$

$$b_2 = 0$$

$$c_2 = -\tfrac{1}{2} \cdot a_2 \qquad \qquad [33]$$

Because the absolute value of no single term is allowed to exceed 1, a_1 must lie between $1/3$ and 1. For $a_1 = 2/3$, all other terms except c_1 are zero. Consequently, a steady state can be generated by a_1 and c_1 alone.

Naturally, one would like to see how such a steady-state solution looks in our usual framework of pure magnetizations M_x, M_y, and M_z. Transformation into Cartesian coordinates follows from Eqs. [8] through [11]:

$$M_x = \sum_{n=1}^{m} \int_0^{2\pi} [(F_n \cdot \cos(2 \cdot n - 1) \cdot \omega \cdot t_e + F_n^* \cdot \sin(2 \cdot n - 1) \cdot \omega \cdot t_e)] d(\omega t_e)$$

$$M_y = \sum_{n=1}^{m} \int_0^{2\pi} [(-F_n \cdot \sin(2 \cdot n - 1) \cdot \omega \cdot t_e + F_n^* \cdot \cos(2 \cdot n - 1) \cdot \omega \cdot t_e)] d(\omega t_e)$$

and

$$M_z = 2 \cdot \sum_{n=1}^{m} \int_0^{2\pi} Z_n \cdot \sin(2 \cdot n - 1) \cdot \omega \cdot t_e d(\omega t_e)$$

where $2 \cdot \tau_e$ is the time between two refocusing pulses, and m is the highest order of configurations included in the calculation. M_z can be calculated from Z_n alone, because the population of Z_n^* is always equal to $-Z_n$. Figure 9 displays some of the steady-state configurations. The solutions of the Bloch equations for the echo time t_e after the refocusing pulse show that the tips of all magnetization vectors for $a_1 = 2/3$, $c_1 = -1/3$ lie on a straight line in the xz plane (Fig. 9b).

The above discussion merely gives solutions consistent with a steady state. It does not tell how such a steady state can be reached or even whether it can be reached at all from a starting point after a 90° excitation pulse where a_1 is 1 and all other configurations are empty. For $a_1 = 2/3$ and $c_1 = -1/3$, one refocusing pulse with $\alpha = 135°$ suffices to generate this particular steady state for all subsequent 90° pulses.

I leave it to the reader to calculate a set of refocusing pulses with different flip angles α such that any of the other steady states described by Eq. [20] are being reached. What is the minimum number of pulses required? What is the maximum echo amplitude attainable in such a steady state?

The numerical solution for a CPMG experiment strongly suggests that the steady-state echo intensity for any refocusing flip angle α is given by $\sin(\alpha/2)$ (3), when α is constant throughout

138

the sequence. For $\alpha = 90°$ an elegant proof can be given by observing invariances like the one given in Eq. [31]. For other values of α, I have not found an elegant proof. Perhaps one of the readers can find one? I would welcome any suggestions.
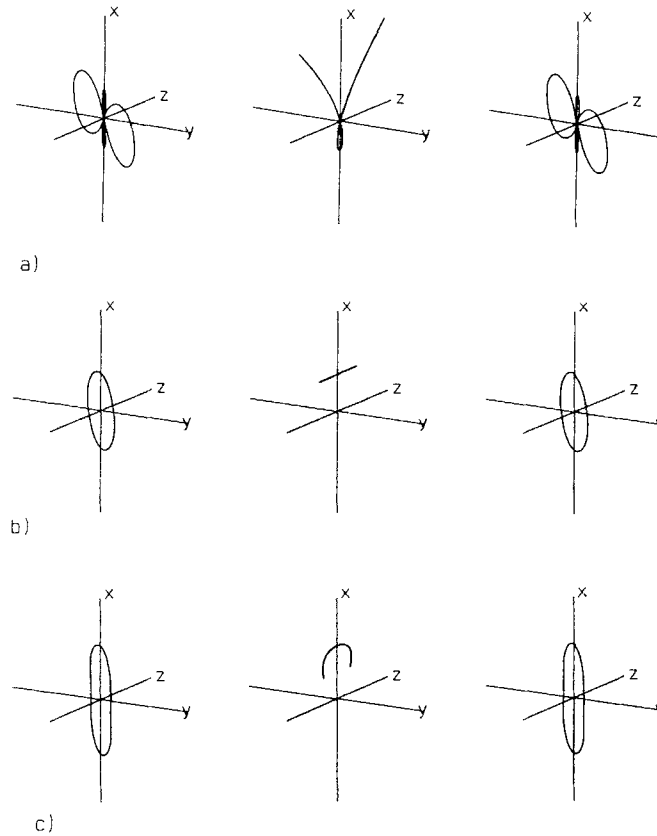

Figure 9. Steady-state configuration before the refocusing pulse (left), at the echo time (middle), and before the next pulse (right) for values of (a) $a_1 = 0.5$, (b) 2/3, and (c) $1/2 * \sqrt{2}$. The configurations at left were created using the parameter equations given in the text; the time evolutions to the echo and to the next pulse were calculated with the Bloch equations.

Figure 9c displays the configuration for $\alpha = 90°$ and $a_1 = \sin(\alpha/2) = \frac{1}{2} \cdot \sqrt{2}$, which is very close to but not equal to the maximum possible intensity. A comparison with the description of M_x, M_y, and M_z given by the Bloch equations (Fig. 2) reveals that the latter description contains irrelevant detail. All important information is contained in the simple description given by Fig. 9c. All the curls seen in Fig. 2 are caused by configurations with higher n, which do not contribute to the steady state itself.

A good way to visualize the time evolution of all states is provided by a stacked plot of the populations of all states F_n and F_n^* for each refocusing period. Experimentally, such a diagram can be generated by terminating the series of refocusing pulses after the nth pulse and watching the amplitudes of the multiple echoes for a time $2 \cdot t_e \cdot n$, which gives the populations of all F_n^* configurations. The populations of all F_n configurations can most easily be measured if the last refocusing pulse is followed by a 180° pulse, which converts all F_n configurations into F_n^* configurations.

Figure 10 shows the results of multi-echo sequences with constant refocusing flip angle α with different boundary conditions and for different values of α. Figure 10a shows that the curls observed in Fig. 2 correspond to the "waves" traveling into configurations with higher n, which become more and more disconnected from the steady state. It is quite interesting to note that,

irrespective of the variation of α and the boundary condition, the flow of magnetization seems to have a strong tendency to evolve in a well-defined manner after a few pulses: a set of configurations remaining in a steady state (which need not necessarily lead to the formation of an echo) and two "magnetization waves" traveling into configurations with higher n. The propagation velocity of these waves is higher for low flip angles than it is for large ones.

The journey of these packages through configuration space strongly resembles the propagation of solitons, traveling waves with constant intensity that occur in dissipative systems. The behavior of magnetization in multi-echo sequences is in fact a very simple and highly informative example to study dissipative structures, as discussed in statistical thermodynamics.
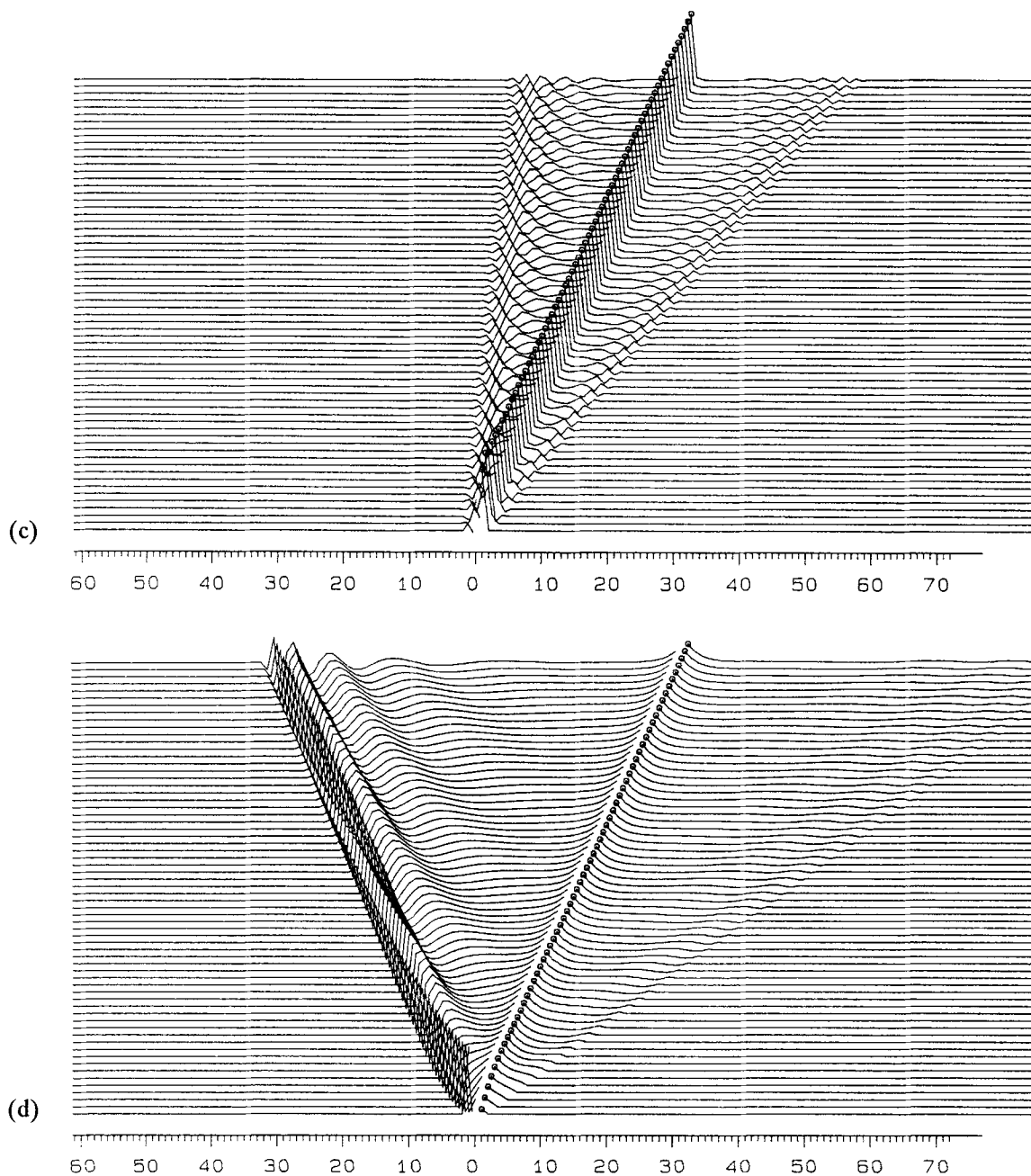

140

(c)

60 50 40 30 20 10 0 10 20 30 40 50 60 70

(d)

60 50 40 30 20 10 0 10 20 30 40 50 60 70
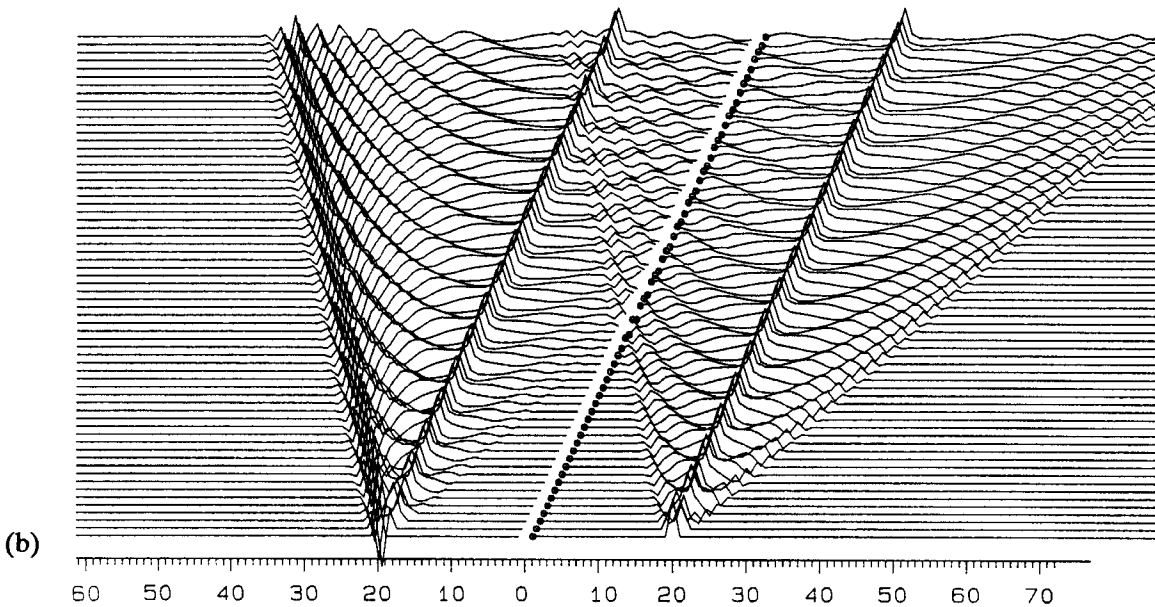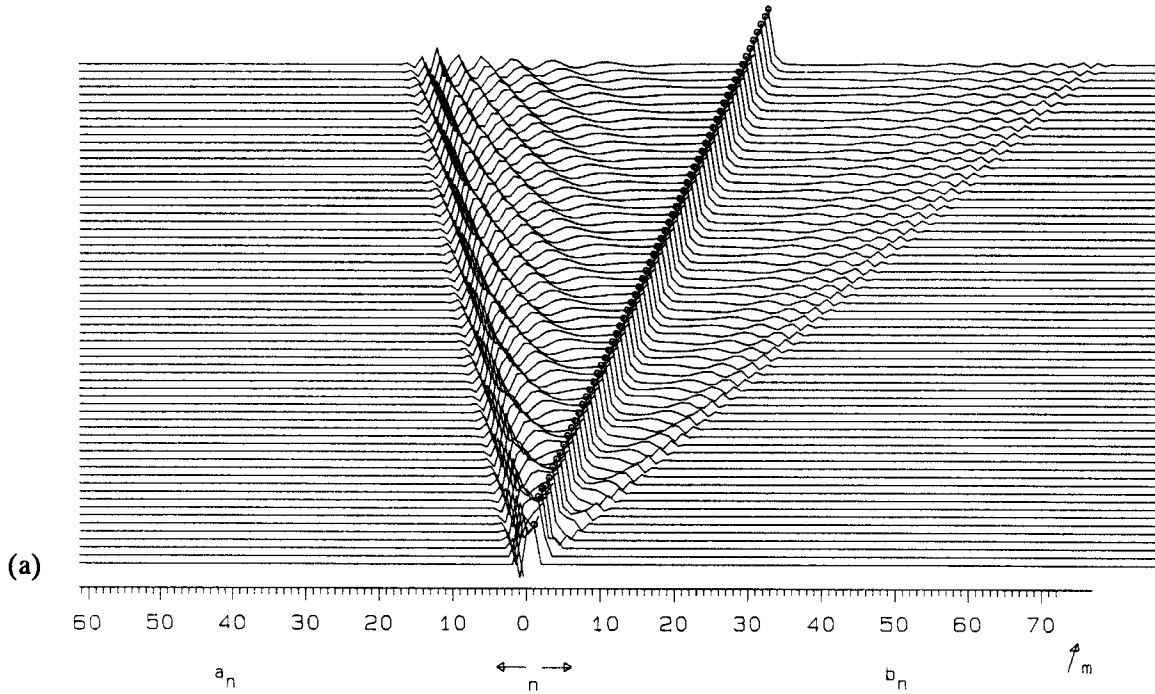
Figure 10. Stacked plot of the evolution of the populations a_n and b_b of all F_n and F_n^* for (a) α = 90°; (b) α = 90° and boundary condition a_{20} = 1, all other configurations empty; (c) α = 150°; and (d) α = 30° The open circles represent the populations leading to echo formation. The stack was shifted one unit to the right for every echo period m. A practical experiment leading to (b) could use the pulse sequence $90° - (39 \cdot t_e) - (90° - 2 \cdot t_e)_n$.

Minor deviations from the periodicity of the multi-echo sequences can be shown to exhibit periodic fluctuations of signal intensities resembling fluctuating chemical reactions (6). To my knowledge, no one has investigated the above observations of magnetic resonance far away from thermal equilibrium in the context of statistical thermodynamics, and such a discussion certainly would be far outside the scope of this paper. I would like to point out, however, that the possibly fascinating but apparently totally useless occupation with such echo sequences has found at least one practical application, namely the DOPE (double phase encoding) sequence for the measurement of extremely slow flow (7).

141

Before ending this section and returning to practical applications of echoes in gradient echo sequences, I would like to point out another connection of multi-echo NMR with an apparently totally unconnected field, namely the theory of cellular automatons (8). Cellular automatons have been used widely but not exclusively in recreational mathematics — most notably in the game, "Life," by A. Conley — to keep students and scientists away from work. A cellular automaton is an entity consisting of discrete cells, whose state is fully defined by the previous history of the states of cells in a defined neighborhood, a definition that fully applies to the evolution of magnetization in configuration space. Traveling "particles" called gliders and steady-state configurations after a few cycles of a more chaotic life are common properties of most nontrivial cellular automatons.

It is a nice exercise on a moderately fast personal computer to create and watch patterns of configurations if more than one or two configurations, as shown in Fig. 10, are "born" with non-zero intensity. The most pleasant presentation is achieved by color-coding the populations on a matrix display.

Please allow me one final thought before going back to more practical matters. Complicated patterns like those in Fig. 10 are created using apparently trivial rotations of vectors. If we were to have no knowledge about the physics of NMR except the results of multi-echo experiments in the form of diagrams like Fig. 10, would we be able to recognize the simplicity of the basic law leading to such intricate patterns? Is there maybe a "truth" much simpler than expected behind other apparently complicated physical phenomena?

SUMMARY

We have reached the end of Part I of this article about echo formation. What looked at first glance like an easy process has turned out to be much more complicated than expected. Still, with the help of the extended-phase-graph algorithm, any multi-pulse experiment can be understood. For most purposes, sketching a diagram like that in Fig. 5 reveals enough relevant information about the occurrence of different kinds of echoes without having to resort to the actual signal calculations using the transition matrix formalism given above.

The examples discussed in this part were chosen to illustrate the large diversity in the behavior of simple spin ensembles and to demonstrate the power of the extended-phase-graph algorithm to deal with such strange phenomena as signal steady states or echo solitons. I hope that in the future, readers will not shy away from the occasionally encountered stimulated echo, but rather regard it as a more basic creature from a much more colorful zoo.

Part II of this article will be dedicated to applying this knowledge about echoes to more practical issues, such as the design of a practical, multi-echo imaging experiment and the understanding of the contrast behavior of gradient-echo imaging sequences, and it will give some advice about the design of multi-pulse sequences in general.

REFERENCES

1. E. L. Hahn, "Spin Echoes," *Phys. Rev.*, **1950**, *89*, 580-594.

2. D. E. Woessner, "Effects of Diffusion in Nuclear Magnetic Resonance Spin-Echo Experiments," *J. Chem. Phys.*, **1961**, *34*, 2057-2061.

3. J. Hennig, "Multiecho Imaging Sequences with Low Refocusing Flip Angles," *J. Magn. Reson.*, **1988**, *78*, 397-407.

4. H. Y. Carr and E. M. Purcell, "Effects of Diffusion on Free Precession in Nuclear Magnetic Resonance Experiments," *Phys. Rev.*, **1954**, *94*, 630-638.

5. S. Meiboom and D. Gill, "Modified Spin-Echo Method for Measuring Nuclear Relaxation Times," *Rev. Sci. Instrum.*, **1958**, *29*, 688-691.

6. A. N. Zaikin, and A. M. Zhabotinsky, "Concentration Wave Propagation in Two-Dimensional Liquid-Phase Self-Oscillating Systems," *Nature*, **1970**, *225*, 535-536.

7. J. Hennig, "Measurements of CSF Flow Using an Interferographic MR Technique Based on the RARE-Fast Imaging Sequence," *Magn. Reson. Imaging*, **1990**, *8*, 543-556.

8. S. Wolfram, "Statistical Mechanics of Cellular Automata," *Rev. Mod. Phys.*, **1983**, *55*, 601-644.